

# A gravity current study within the Palma de Mallorca basin

Daniel MARTÍNEZ and Joan CUXART

Universitat de les Illes Balears  
Departament de Física  
dani.martinez@uib.es

(Received 24 April 2007; received in revised form 15 June 2007; accepted 18 June 2007)

## ABSTRACT

An analysis of a katabatic flow is made through data provided by a high resolution mesoscale simulation of the isle of Majorca in the western Mediterranean sea. It is found that a quasi-steady state is reached in the second part of the night and that the katabatic flow interacts with a cold pool formed at the end of the slope, in the center of the Palma basin. The application of a two-layer model following the framework set out in Mahrt (1982) shows that the main term of the momentum budget equation is the buoyancy force, which is generally balanced by the stress divergence and the advection term. The entrainment at the top is small and the scale analysis shows that the flow is in a shooting regime, in agreement with the hydraulic theory. Finally, an oscillatory behaviour of the wind speed and potential temperature is well correlated with the changes in the slope angle and it is adapted with the waves generated above in the lee side of the mountain.

**Key words:** Katabatic wind, Mesoscale model, Stable boundary layer, Hydraulic model.

## Estudio de una Corriente de Gravedad en la Cuenca de Palma de Mallorca

### RESUMEN

Se realiza el análisis de un viento catabático utilizando los datos procedentes de una simulación mesoescalar de alta resolución en la isla de Mallorca, situada en el Mar Mediterráneo Occidental. El régimen casi-estacionario es alcanzado durante la segunda mitad de la noche y la corriente catabática interacciona con una piscina de aire frío que se forma al pie de la pendiente, coincidiendo con el centro de la cuenca de Palma. La aplicación de un modelo de dos capas según el marco establecido por Mahrt (1982) indica que el término principal de la ecuación de balance para el momento es la fuerza de flotabilidad, la cual se encuentra generalmente compensada por la divergencia del flujo del momento y el término de advección. La intrusión de aire en la cima de la capa catabática es pequeña y un análisis de escala indica que la corriente se encuentra en un régimen disparado, de acuerdo con la teoría hidráulica. Finalmente, en la simulación aparece un comportamiento oscilatorio para la velocidad del viento y la temperatura potencial bien correlacionado con los cambios de inclinación a lo largo de la pendiente. Estas oscilaciones se adaptan a las ondas generadas a sotavento de la montaña.

**Palabras clave:** viento catabático, modelo de mesoescala, capa límite atmosférica, modelo hidráulico.

## 1. INTRODUCTION

The interaction between the atmospheric boundary layer and the earth's topography is far to be simple. The presence of mountains, valleys, slopes and

the rest of topographic systems leads to a list of local meteorological phenomena which include, for example, the formation of cold pools in the center of the basin (Clements et al 2003), the presence of valley winds and their relation with the synoptic flow depending on the main forcing mechanism (Whiteman and Doran 1993), slope flows and other kinds of low-level jets (Cuxart 2007 in press).

Under stably stratified conditions, when the pressure gradient is weak and the sky is cloudless, turbulence mixing is inhibited and large temperature gradients are formed due to the non uniform surface cooling. Depending on the spatial and time scales, the quasi-horizontal motions generated in this way can evolve to a steady situation, affecting the local climate. Moreover, the vertical transport from the surface to the free atmosphere is mainly driven by these flows. Thus, it is necessary to analyze how they function and organize over complex terrain.

For the gravity flows, several studies have been performed focusing on their stationary vertical structure (Prandtl 1942; Stiperski et al 2007) or on their bulk evolution with time (Fleagle 1950; McNider 1982). In the latter case, the study can be extended to the along-slope evolution after assuming steady-state (Ball 1956; Manins and Sawford 1979). Those studies found analytical solutions from a balance of two or three dominant terms in the momentum and heat budget equations. Mahrt (1982) made a detailed scale analysis and a critical study of all the possible approximations. He provided a framework to study real katabatic flows, as in Heinemann (2002) or Renfrew (2004), that used it to investigate the dynamics of katabatic flows over Greenland and the Antarctica, respectively. Haiden and Whiteman (2005) applied it to a katabatic flow measured in mid-latitudes.

The observational study of the downslope flows is not straightforward. A practical complementary tool is mesoscale modelling. In this work, high-resolution mesoscale simulations are performed to analyze the katabatic flow developed over a gentle slope during one stable night in Majorca island. In section 2, a description of the island and the region where the katabatic wind takes place is made. Section 3 is devoted to the main characteristics of the flow, while section 4 focuses on the analysis of the current according to the proposals of Mahrt (1982) or the more recent work of Renfrew (2004). Finally, a summary of the results is given in section 5.

## 2. SITE DESCRIPTION

Majorca is the largest island of the Balearic archipelago, located in the western Mediterranean sea, 200 km towards west from the east coast of the Iberian Peninsula. It has a characteristic size of 100 km and a large mountain range at its north-western side (*serra de Tramuntana*), with an average height of 700 m above sea level (ASL) and a maximum peak that reaches 1450 m ASL. Another lower and discontinuous mountain range is present at the south-eastern side (*serra de Llevant*), with an average height of 300 m ASL. At the central part of the island, the terrain is mainly flat but has a 500 m-high mountain called Randa.

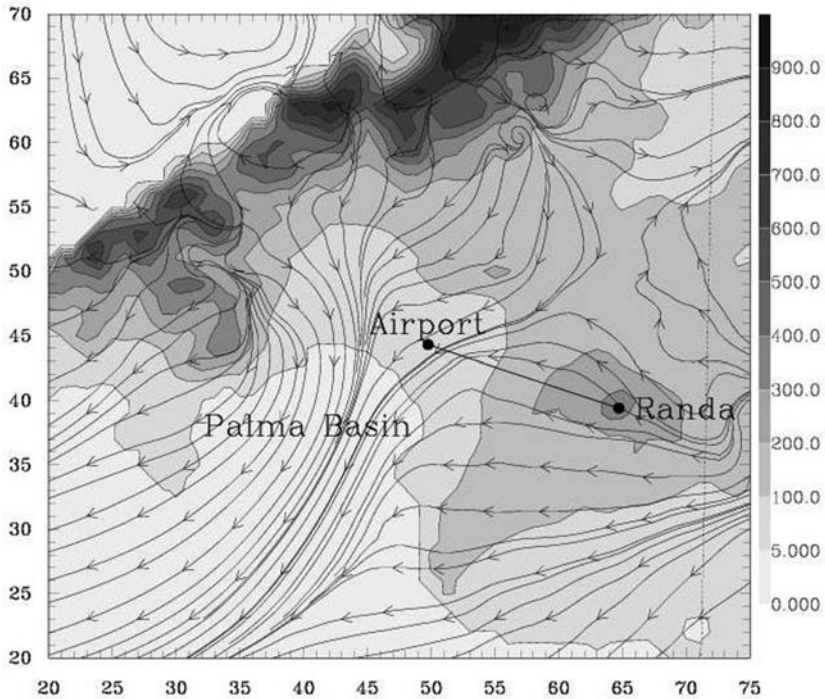


**Figure 1.-** Streamlines at 30 m (AGL) over topography (in m) implemented by the model at 0400 UTC within Palma basin. Axis labels indicate the distance from the origin of the inner domain (in km). Line corresponds to the cross section used to study the downslope flow in further figures.

The topographical configuration of *serra de Tramuntana*, the elevated platform at the center and Randa mountain form the Palma basin at the western side of the isle. The basin is almost closed with the only exit to the sea through the southern side. The south-eastern part of the basin contains a quasi-bidimensional gentle slope parallel to the sea coast of almost constant angle. The line chosen to study the wind dynamics of the katabatic wind is between the Randa peak and the airport, which is found at the center of the basin (Fig. 1). It describes, firstly, a steep part of 100 m in 1 km (a 10% slope), then 50 m in 4 km (a 1.25% slope) and finally the drop of 200 m in 8 km to the center of the basin (a 2.5% slope). The terrain is agricultural, with fields of olive, carob and almond trees and some small pine woods.

### 3. DESCRIPTION OF THE FLOW

To perform this study, the Meso-NH model of the French community has been used (Lafore et al 1998). Two domains are chosen, the largest one with a resolution of 5 km and the inner one of 1 km, covering only Majorca. The initial and boundary conditions are provided by the European Center of Medium-range Weather Forecasts (ECMWF) analyses. The simulation runs from 1200 UTC on

January 5th 1999 to the dawn of the next day, thus covering completely the 15-hour-long night. It has been run on the ECMWF supercomputers. Only plots of the inner domain will be shown in this work, mainly at 0400 UTC, which is considered a time representative of the quasi-state situation of the second part of the night.

The vertical resolution is very high near the ground, to be able to capture all the details of the low level flows: close to 3 m in the surface layer, with a stretching factor that leads the resolution to about 8 m at 500 m ASL and to 600 m at the top of the model (6200 m ASL). Such a fine vertical resolution implies very short timesteps (below 2 s), especially at mountain slopes.

The synoptic situation for the night of 5-6 January 1999 was characterized by a weak gradient of pressure. The archipelago was very close to the center of a winter high pressure system, with the flow coming from the southeast (of about  $4 \text{ m s}^{-1}$  over the sea at 10 m), thus parallel to the slope direction. The skies were cloudless and the humidity was low. The situation was steady at the synoptic scale during all the run.

With this configuration, the centre of the island became an area of minimum wind speeds, able to develop freely motions determined by the topographical configuration. In particular, at low levels, the centre of the Palma basin accumulates the cold air transported by the flows that arrive from all the surrounding slopes. The cold pool is impelled to the sea driven by the pressure gradient that results from the warmer air above the water in the Palma bay. Fig. 1 shows the streamlines distribution at 30 m above ground level (AGL) within the Palma basin when motion is influenced by the complex terrain.

Over the line from Randa peak to the airport, a katabatic flow is well developed two hours after the sunset (1640 UTC). This slope, which has a length of 10 km and a drop of 500 m, is well represented by the model topography, although the height of the mountain peak is underestimated. Fig. 2 shows the horizontal wind vector at 30 m AGL on the topography implemented by the model at 1900 UTC, 0000 UTC and 0400 UTC. Over the slope, gravity flow turns to the right and then to the left but sustaining the downslope direction as the main wind component during the night. As the flow arrives to the airport, it turns to the cross-slope direction and joints with the land-to-sea flow. The wind direction at the airport remains nearly constant during the whole night (NE).

In Fig. 3 the wind speed and potential temperature fields over the line Randa-airport at 0400 UTC are shown. A maximum of wind is generated downslope of the Randa Mountain. At the change of slope the maximum is found at about 80 m above the surface and when the slope becomes steeper, the wind accelerates again, with a maximum of about  $5 \text{ m s}^{-1}$  at 50 m AGL. When the downslope wind reaches the cold air in the basin it seems to split, with some air flowing close to the surface and the upper air above the cold area (300 m AGL). Renfrew (2004) found an elevated jet as the tail end of a part of the katabatic flow that rides over the cold air of the ice shelf. In the slope studied here, the temperature takes lower values at the parts where the slope is less steep. This structure would be in support of a layered structure of potential temperature over the valley created by the converged flows according to their final potential temperature. Here, each katabatic flow would contribute to air accumulation at its arriving level, except for the coldest air that would flow close to the surface. Mahrt et al (2001) found a similar behaviour at a very small scale in a gully during CASES-99.

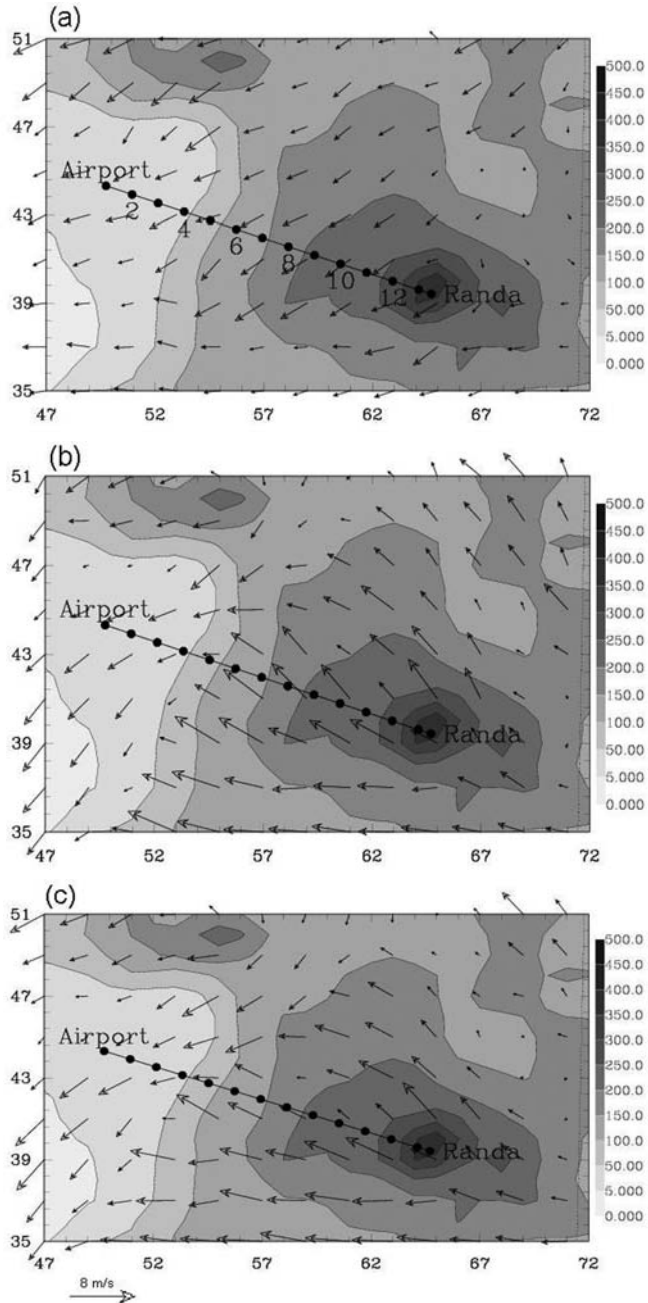


**Figure 2.-** Horizontal wind vectors at 30 m (AGL) over topography (in m ASL) implemented by the model at (a) 1900 UTC, (b) 0000 UTC and (c) 0400 UTC. Bold line refers to the same cross section as in Fig.1. Dots indicate the points where variables from the model have been interpolated. Above these lines, a maximum wind vector is plotted with a windspeed of  $8 \text{ m s}^{-1}$ .

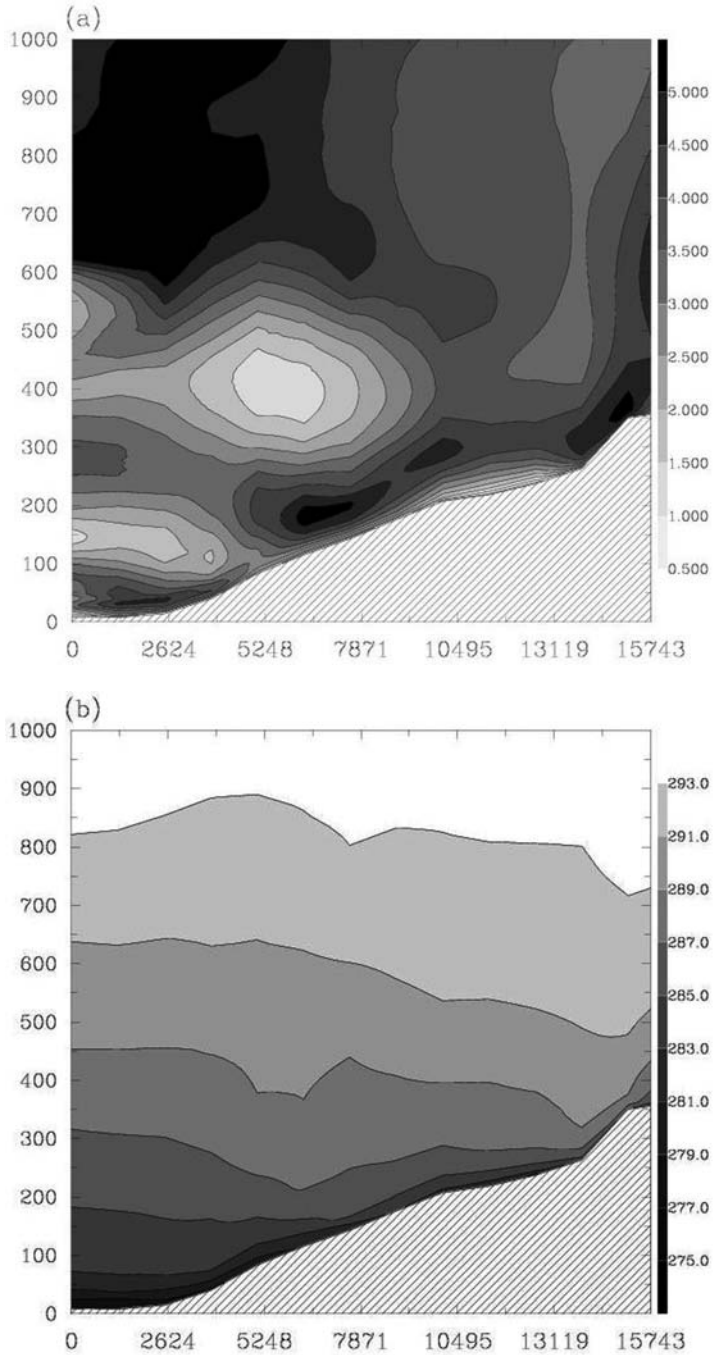


**Figure 3.-** Vertical cross section at 0400 UTC following the line in Fig. 2. (a) Wind speed (in  $\text{m s}^{-1}$ ) and (b) Potential temperature (in K). Axis labels in meters. Taken from Cuxart et al 2007.

Although this picture is quite stationary during the night, there is certain temporal variability point to point. For the point 8 in Fig. 2 (considering the Airport the point 1 and Randa peak, the point 14), the maximum of the wind can take values between 3 and 7 m s<sup>-1</sup>, and its height oscillates between 20 and 100 m, being the more probable values around 40 m. The thermal stability -in average- below the jet nose is almost constant during the night (about 3 K in 40 m), and is weaker above (1 K in 100 m) and oscillating.

#### 4. KATABATIC FLOW DYNAMICS

In a rotated coordinate system, the momentum equation for a katabatic flow over a slope with a constant inclination angle  $\alpha$  can be written as (Mahrt 1982):

$$\frac{Du}{Dt} = -\frac{1}{\rho_0} \frac{\partial p}{\partial x} + g \frac{\Delta\theta}{\theta_0} \sin \alpha + fv - \frac{\partial(\overline{w'u})}{\partial z} \quad (1)$$

where shallow convection and "quasi-hydrostatic" approximations have been made, in which the hydrostatic equilibrium is present only for motions perpendicular to the ground (Mahrt 1982; Haiden 2003). Here,  $\Delta\theta$  is defined as the deficit of potential temperature and  $\theta_0$  and  $\rho_0$  represent the basic state potential temperature and air density representative of the air outside the gravity flow. The velocities  $u$  and  $w$  are referred to the rotated axes, tangent and normal to the slope, respectively.

Following Renfrew (2004), a two-layer model is assumed consisting of a katabatic layer as the lower one and a quiescent layer at higher level. A vertical integration of the momentum budget (1) from the ground to the katabatic-layer top ( $h_k$ ), assuming that the temperature deficit and wind speed vanish at the top of the layer and at the surface, respectively, yields:

$$\begin{aligned} \frac{\partial u_k}{\partial t} = & - \left( u_k \frac{\partial u_k}{\partial x} + w_k \frac{u_h - u_k}{h_k} \right) + g \frac{\Delta\theta_k}{\theta_0} \alpha - \frac{gh_k}{\theta_0} \frac{\partial \Delta\theta_k}{\partial x} - \frac{g\Delta\theta_k}{\theta_0} \frac{\partial h_k}{\partial x} + fv_k - \\ & - \frac{(\overline{w'u})_h - (\overline{w'u})_{sfc}}{h_k} = F_{adv} + F_b + F_{\Delta\theta} + F_h + F_{cor} + F_{div} \end{aligned} \quad (2)$$

where small angle slopes are considered ( $\sin\alpha \sim \alpha$ ,  $\cos \alpha \sim 1$ ). Here,  $u_k$ ,  $w_k$  are katabatic-layer average velocities,  $u_h$  is the velocity at the top of the layer,  $\theta_0$  is a reference potential temperature and it is taken here as the value at the top of the layer,  $\Delta\theta_k = \theta_0 - \theta_k$  is the katabatic-layer potential temperature deficit,  $g$  is the gravitational acceleration,  $f$  is the Coriolis parameter, and  $(\overline{w'u})_{sfc}$ ,  $(\overline{w'u})_h$  are the vertical turbulent u-momentum fluxes at the surface and at the top of the layer. The Lagrangian derivative has been expanded and the cross-slope variation of  $u_k$  has been neglected.

Equation (2) contains the different forcing terms involved in the momentum equation:  $F_{adv}$  refers to the total advection,  $F_b$  is the buoyancy term that, by definition, is supposed to be the source of the katabatic flow,  $F_{\Delta\theta}$  and  $F_h$  are referred to as the thermal-wind terms (Mahrt 1982), which are relevant if the layer depth and the katabatic potential temperature deficit vary along the slope.  $F_{cor}$  is related with the Coriolis force and  $F_{div}$  represents the divergence of turbulent vertical flux term and is related with the surface drag and the entrainment at the top.

To apply the analysis to our case, a definition of the top of the katabatic layer is required. Due to the relative unsteadiness of the regime and its spatial variability, here  $h_k$  is considered to be the height of temperature inversion related with the maximum wind generated by the katabatic flow.

#### 4.1. KATABATIC-LAYER AVERAGE VALUES

The time-averaged values along the slope for the relevant parameters of the above formulation have been computed using the simulation outputs from two periods of the night. The first one starts two hours after the sunset (1900 to 2000 UTC) and the second one finishes three hours before sunrise (0200 to 0400 UTC). Comparing the results from both data sets it is possible to find out the evolution of the katabatic layer along the night. Since the flow at the end of the slope (points airport to 5 in Fig. 2) merges with the downvalley wind, a different behaviour for the bulk variables is expected in these points.

The main remarks found are summarized as follows. Over the slope, the depth of the katabatic layer increases and the potential temperature stays approximately constant with time. Over the plain, where the cold air is accumulated, the layer cools around 3 K and its depth decreases. Moreover, the cross-slope velocity  $v_k$  changes significantly during the night, except at the plain, confirming the turning feature of the slope wind and the constancy of the land-to-sea flow within the basin (Fig. 2).

An oscillatory behaviour along the slope (which becomes more relevant at the second period) is detected with the average velocity  $u_k$  (Fig. 6), whose maximum values match with potential temperature crests and both are well correlated with the changes of the slope. The slope-relative vertical wind component  $w_k$  (which is approximated to the vertical component) also alternates negative and positive values along the slope in agreement with the oscillatory distribution during the second period (0200-0400 UTC). Finally, the locations with a higher downslope velocity  $u_k$  also have high values of surface turbulence flux  $(w'u')_{sfc}$  due to an increment of the wind shear close to the surface.

The momentum flux is, in general, one order of magnitude greater at the surface than at the top of the katabatic flow. This situation suggests that entrainment is not relevant and only surface friction can be considered, like the flow described by Ball (1956). In Renfrew (2004), entrainment arose as important as surface drag because a quiescent upper layer leads to an important windshear at the top of the flow and the roughness length over ice is very low, therefore

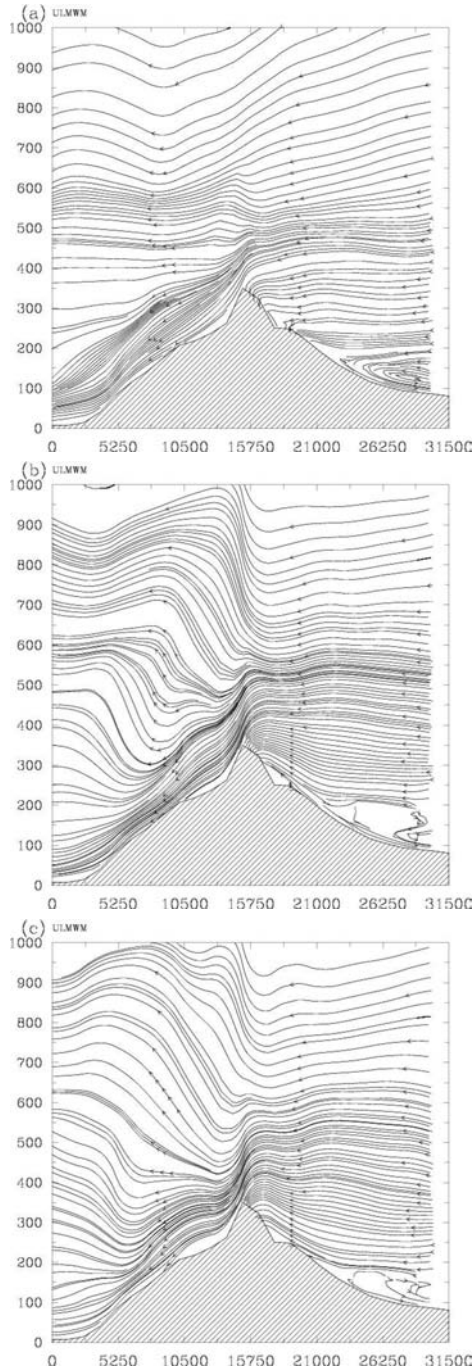


**Figure 4.-** Vertical stream lines at the Randa Mountain following the direction of the line in Fig. 2 at (a) 1900 UTC, (b) 0000 UTC and (c) 0400 UTC. Axis labels in meters. Taken from Cuxart et al 2007.

diminishing the difference between these two factors. For Manins and Sawford (1979), the dominant retarding stress is the one related with the entrainment due to the interfacial mixing. However, in present study, the wind velocity is significant above the katabatic layer and it has the same direction than the slope flow. Therefore, less shear generation of turbulence is produced in respect to a quiescent layer above. This lack of mixing with the upper layers does not allow the katabatic air to get warmer or to lower its speed as much, probably resulting in very well defined cold and relatively fast flows. This issue requires more sounded investigation with the support of observations.

Fig. 4 shows the streamlines over the Randa mountain at three different moments of the night. The wind direction is modified by the mountain, leading to a steady configuration that seems to strengthen with time. Wind speed increases near the mountain peak and close to the points where the angle slope changes. The same pattern can be inferred from the field of potential temperature  $\theta$  (not shown). Terrain-generated gravity waves are stationary relative to the ground surface (Nappo 2002) like the oscillatory behavior detected in the present katabatic flow. The estimated Froude number for the ambient flow ( $Fr = U/Nh$ , with  $N = 0.04 \text{ s}^{-1}$ ,  $U = 4 \text{ m s}^{-1}$  and  $h = 300 \text{ m}$  for the average Randa mountain height), is about 0.3. Following Poulos et al (2000), this value leads to a situation where the downslope phase of the mountain wave couples with the katabatic flow, enhancing its speed. Furthermore, the relation between downslope windspeed and the slope suggests that the katabatic wind is modified by changes of the angle and by the interaction with the mountain wave, propagating the perturbations upwards and modulating the flow in the first thousand of meters above the ground.

The oscillatory behaviour described here has been partially confirmed by experimental data using the NOAA IR imagery. The radiative surface cooling rate computed between 1900 UTC and 0400 UTC has been compared with the estimated outputs from the two available NOAA images (1846 UTC and 0405 UTC). In both cases, the points with the greatest surface cooling rate coincide with those with a weak wind strength (Cuxart et al 2007).

## 4.2. FORCING TERMS FROM MOMENTUM EQUATION

Fig. 5 illustrates the forcing terms of the downslope momentum budget from equation (2). The buoyancy force  $F_b$  is balanced by momentum flux divergence  $F_{div}$  (specially at the beginning of the night) and the advection term  $F_{adv}$ . The latter does not always slow the flow as it changes its sign along the slope. The thermal-wind terms  $F_{\Delta\theta}$  and  $F_h$  are generally small and the Coriolis term  $F_{cor}$  is irrelevant due to the small spatial scale of the phenomena.

Finally,  $F_{res}$  is the residual of equation (2) that also includes the Eulerian acceleration (which only takes values of around  $\sim 10^{-7} \text{ m s}^{-2}$ ). The sign of the residual is opposite to  $F_{adv}$  in almost every point, suggesting that the estimation of the total advection term is the main source of error. To improve the results, three-dimensional effects should be considered to represent better the advection term.

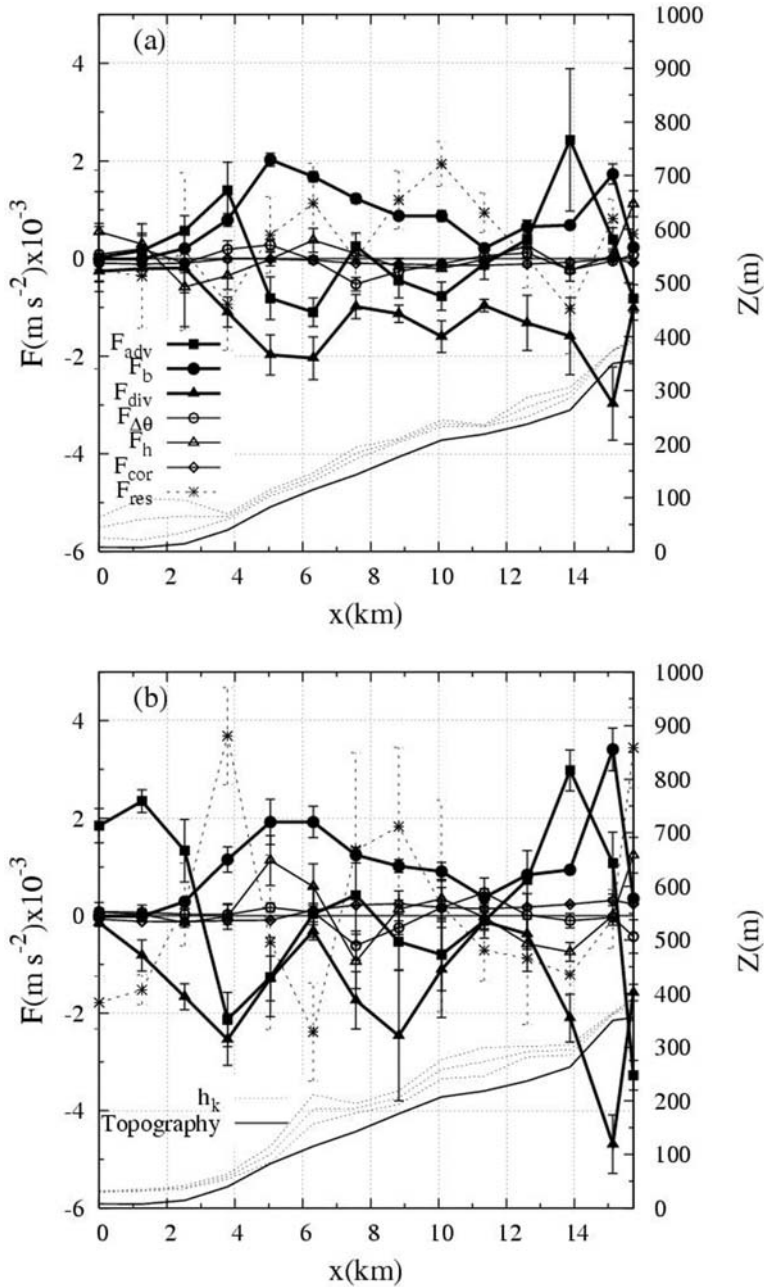


**Figure 5.-** Mean forcing terms from the downslope momentum equation for the katabatic layer along the slope following the line in Fig. 2 (in  $\text{m s}^{-2}$ ). Time-averaged values and standard deviation are plotted for two different periods of the night: (a) 1900-2000 UTC and (b) 0200-0400 UTC period. The average katabatic-layer height  $h_k$  and the standard deviation (in m) are also plotted but relative to the topography line. Taken from Cuxart et al 2007.

These results are in agreement with Mahrt (1982), who showed that gravity flows can be generally approximated by a balance between buoyancy acceleration and downslope advection of weaker momentum or/and the turbulent transport term. Such flows coincide with a Froude number ( $Fr = (u_k^2 q_0)/(g\Delta\theta h_k)$ ) greater than one, as in present case, where  $Fr > 1$  along the slope (not shown) and the katabatic wind can be considered a *shooting* flow in terms of the hydraulic theory.

The point located at the upper part of the longer slope (about km 11) has a very small contribution of all the forcing terms. From this point on, the buoyancy term grows downslope. It can be considered the origin of the buoyancy-driven flow. Another "singular" point is where the katabatic flow meets the downvalley flow in the second period (km 6). Here, the buoyancy force is not balanced by any forcing term except for the residual, attributable to non-2D effects. Also, the thermal wind terms ( $F_{\Delta\theta}$  and  $F_h$ ) are higher around this point due to the relevant changes of the vertically averaged potential temperature and the layer depth in that place.

### 4.3. MAHRT'S ANALYTICAL SOLUTION

Mahrt (1982) presented a simple solution for downslope momentum equation (2) to cases where main terms are  $F_b$ ,  $F_{div}$  and  $F_{adv}$ . Neglecting the rest of forcing terms and assuming constant  $h_k$ , downslope wind speed can be written as:

$$u_k = \left[ u_e^2 \left[ 1 - \exp\left(\frac{-x}{L_e}\right) \right] + u_k^2(0) \exp\left(\frac{-x}{L_e}\right) \right]^{1/2} \quad (3)$$

$$u_e \equiv \left[ \frac{h_k g (\Delta\theta/\theta_0) \sin\alpha}{(C_D + k)} \right]^{1/2} \quad L_e \equiv \frac{h_k}{C_D + k}$$

where  $u_k(0)$  is the katabatic layer mean velocity at some arbitrary point on the slope;  $u_e$  is the solution for an *equilibrium flow*, a case where buoyancy acceleration only balances with turbulence term; and  $L_e$  is a length scale related with the distance needed for the flow to adjust to the equilibrium case.  $C_D$  and  $k$  are the drag and the entrainment or mixing coefficients, respectively, and here are calculated through the vertical turbulent flux of momentum at the surface and at the top of the katabatic layer:

$$C_D = - \frac{(\overline{w'u})_{sfc}}{u_k^2}; \quad k = \frac{(\overline{w'u})_h}{u_k^2} \quad (4)$$

Fig. 6 illustrates the evolution of  $u_k$  along the slope for points where the buoyancy term is dominant (from the point located close to km 11, which is

considered the origin of the katabatic wind, to km 4 in Fig. 5). Therefore,  $u_k(0)$  represents the vertically averaged velocity at the upper point of the area chosen. To apply the solution (3), it is necessary to assume that the parameters  $u_e$  and  $L_e$  are constant. A representative value for all the points has been estimated from the simulation for both time intervals analyzed (1900-2000 UTC and 0200-0400 UTC). Table 1 summarizes the values for the parameters needed to plot fig. 6. The resulting length scale  $L_e$  is similar to the downslope length scale and, consequently, the katabatic flow cannot reach the *equilibrium regime*.

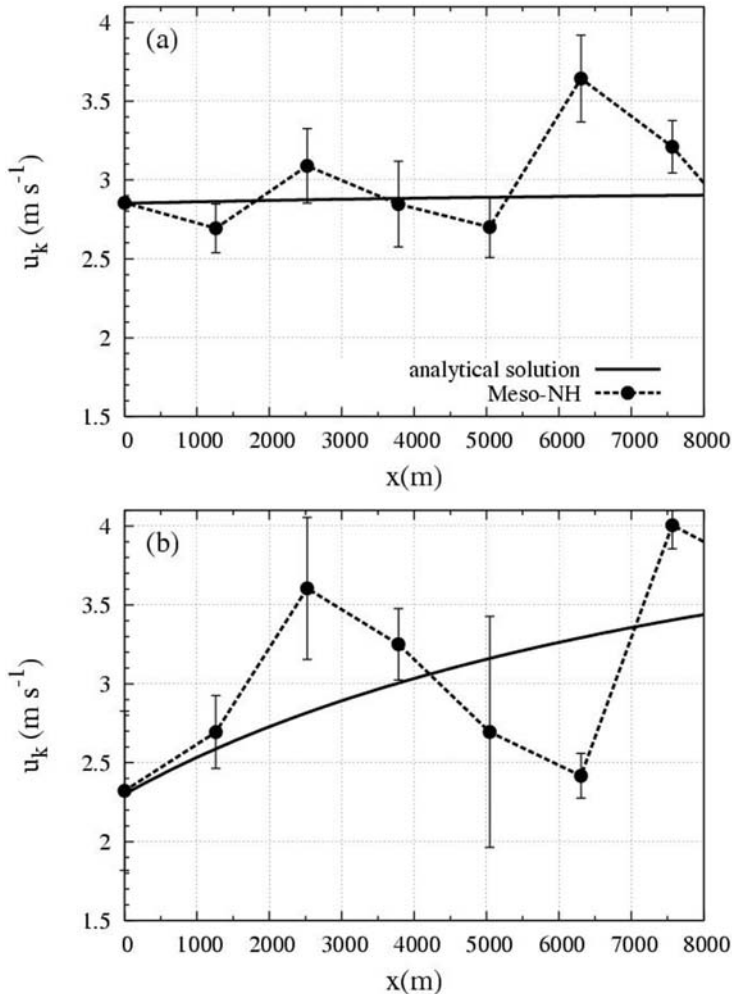


**Figure 6.-** Solution for the downslope momentum equation (3) in the simple case of a *shooting* flow assuming constant  $h_k$  for points over slope where buoyancy term is dominant. X-axis indicates the downslope distance respect to the 10th point (beginning in the airport) in Fig. 2. Time-average wind speed  $u_k$  and standard deviation from simulation is also plotted. (a) 1900-2000 UTC and (b) 0200-0400 UTC.

**Table 1.-** Values used for the parameters present in the analytical simple solution for downslope momentum equation (3) in the case of a shooting flow.

	1900-2000 UTC	0200-0400 UTC
$C_D + k$	0.004	0.004
$h_k$	30 m	40 m
$\Delta\theta$	1 K	1.5 K
$\theta_0$	283 K	283 K
$\sin\alpha$	0.033	0.033
$u_k(0)$	2.83 m s <sup>-1</sup>	2.30 m s <sup>-1</sup>
$u_e$	2.93 m s <sup>-1</sup>	4.14 m s <sup>-1</sup>
$L_e$	7500 m	10000 m

The analytical simplified solution reproduces the tendency of the slopewind velocity from the simulation, which increases with the slope in both periods. The increasing of  $u_k$  is bigger during 0200-0400 UTC, but  $u_k(0)$  is smaller. However, the solution (3) is very sensitive to changes in the parameters. For instance, arbitrary changes in the origin point  $u_k(0)$  or in the estimation of  $h_k$ , may lead to a simplified solution with a different tilt, losing the similarity with the tendency from the simulation results.

Since the oscillatory behavior of  $u_k$  is assumed to be related with terrain-generated gravity flows, the simplified solution cannot reproduce it. Besides, for the katabatic flow simulated,  $h_k$  is not constant and thermal wind terms are not smaller enough to be neglected in some specific points, specially during time interval 0200-0400 UTC.

## 5. CONCLUSIONS

The katabatic wind studied here has been analyzed taking into account the topographical characteristics of the island, which has a complex flow pattern in the nighttime. When the synoptic wind is weak, the island becomes an area where locally generated winds prevail. The mesoscale simulation, performed at a high vertical resolution, allows to inspect many details of the gravity flow and its interaction with higher scales (i.e., basin flows). Although around 5 hour after the sunset all the patterns are almost stationary, there is some temporal variability that remains until dawn.

With an average depth of 40 m and a mean layer velocity of 3 m s<sup>-1</sup>, the descending wind twists around the downslope direction and the lower part adapts to the general configuration within the basin. The changes in the slope angle downhill are well correlated with those in the wind speed and the potential temperature near the ground, determining their spatial distribution and leading to steady oscillations confirmed by the inspection of two NOAA images.

The analysis of the terms of the momentum budget shows that buoyancy force is generally balanced by the momentum flux divergence and, in some cases, by the total advection. Latter term is not well parameterized since the two-layer model reduces the system to a two dimensional problem. Furthermore, the entrainment is not a relevant factor for this flow, that can be adapted with the one above, especially with waves generated by the mountains.

Both scale analysis and hydraulic theory show that katabatic wind is in a *shooting* regime. The increment of mean katabatic-layer velocity  $u_k$  along the slope is predicted by a simple analytical solution and accomplished by the simulation. However, the steady wind oscillations cannot be explained by the katabatic theory since they are related with the mountain-generated waves. All these features should be further investigated through direct observational work.

## 6. ACKNOWLEDGEMENTS

The European Center for Medium-range Weather Forecasts (Reading, UK) is acknowledged for the access to its computing facilities, through the intermediation of the Spanish Met. Service (INM). Many thanks as well to the Centre National de Recherches Météorologiques (Toulouse, France) for their support in the use of the Meso-NH model. Maria Antonia Jiménez is also acknowledged for the performance of the simulation. This work has been partially funded by the research project REN2003-09435/CLI of the Spanish Ministry of Research, and by a Special Project of the Government of the Balearic Islands.

## 7. REFERENCES

- BALL, F. K. (1956). The theory of strong katabatic winds. *Aust. J. Phys.*, 9, 373-386
- CLEMENTS, C. B., C. D. WHITEMAN & J. D. HOREL (2003). Cols air poll structure and evolution in a mountain basin: Peter Sinks, Utah. *J. Appl. Meteor.*, 42, 752-768.
- CUXART, J. (2007). Nocturnal Basin Low-Level Jets: an integrated study. *In Press to Acta Geophysica*.
- CUXART, J., M. A. JIMÉNEZ & D. MARTÍNEZ (2007). Nocturnal Meso-Beta Basin and Katabatic Flows on a Midlatitude Island. *Mon. Wea. Rev.* 135, 918-932.
- FLEAGLE, R. G. (1950). A theory of air drainage. *J. Atmos. Sci.*, 60, 1632-1635.
- HADEN, T. & C. D. WHITEMAN (2005). Katabatic flow mechanisms on a low-angle slope. *J. Appl. Meteor.*, 44, 113-126.
- HEINEMANN, G. (2002). Modelling and observations of the katabatic flow dynamics over Greenland. *Tellus*, 54A, 542-554.
- LAFORE, F. P., J. STEIN, N. ASENCIO, P. BOUGEAULT, V. DUCROCQ, J. DURON, C. FISHER, P. HÉREIL, P. MASCART, J. P. PINTY, J.-L. REDELSPERGER, E. RICHARD & J. VILÁ-GUERAU DE ARELLANO (1998). The Meso-NH atmospheric simulation system. Part I: Adiabatic formulation and control simulation. *Ann. Geophys.*, 16, 90-109.

- MAHRT, L. (1982). Momentum balance of gravity flows. *J. Atmos. Sci.*, 39, 2701-2711.
- MAHRT, L., D. VICKERS, R. NAKAMURA, M. R. SOLER, J. L. SUN, S. BURNS & D. H. LENDSCHOW (2001). Shallow drainage flows. *Bound. -Layer Meteorol.*, 101, 243-260.
- MANINS, P. C. & B. L. SAWFORD (1979). A model of katabatic winds. *J. Atmos. Sci.*, 36, 619-630.
- MCNIDER, R. T. (1982). A note on velocity fluctuations in drainage flows. *J. Atmos. Sci.*, 39, 1658-1660.
- NAPPO, C. L. (2002). *An Introduction to Atmospheric Gravity Waves*. Academic Press, 276 pp.
- PRANDTL, L. (1942). *Strömungslehre*. Verlag Vieweg und Sohn., 382 pp.
- POULOS, G. S., J. E. BOSSERT, T. B. MCKEE & R. A. PIELKE (2000). The interaction of Katabatic Flow and Mountain Waves. Part I: Observations and Idealized Simulations. *J. Atmos. Sci.*, 57, 1919-1936.
- RENFREW, I. A. (2004). The dynamics of idealized katabatic flow over a moderate slope and ice shelf. *Quart. J. Roy. Meteor. Soc.*, 130, 1023-1045.
- STIPERSKI, I., I. KAVCIC, B. GRISOGONO & D. R. DURRAN (2007). Including Coriolis effects in the Prandtl model for katabatic flow. *Quart. J. Roy. Meteor. Soc.*, 133, 101-106.
- WHITEMAN, C. D. & J. D. DORAN (1993). The relationship between overlying synoptic-scale flows and winds within a valley. *J. Appl. Meteor.*, 32, 1669-1682.